686 *Inorg. Chem.* **2010**, *49*, 686–694
DOI: 10.1021/ic901962k

Inorganic Chemistry
Article

Pseudotetragonal Structure of $Li_{2+x}Ce_x^{3+}Ce_{12-x}^{4+}F_{50}$: The First Mixed Valence Cerium Fluoride

Guillaume Renaudin,*[,†,‡] Belto Dieudonné,[‡,§] Daniel Avignant,[‡,§] Elise Mapemba,[‡,§] Malika El-Ghozzi,[‡,§] Solène Fleutot,[∥] Hervé Martinez,[∥] Radovan Černý,[⊥] and Marc Dubois[‡,§]

[†]*Clermont Université, ENSCCF, Laboratoire des Matériaux Inorganiques, BP 10448, F-63000 Clermont-Ferrand, France,* [‡]*CNRS, UMR 6002, F-63177 Aubière Cedex, France,* [§]*Clermont Université, Université Blaise Pascal, Laboratoires des Matériaux Inorganiques, BP 10448, F-63000 Clermont-Ferrand, France,* [∥]*Université de Pau et des Pays de l'Adour, IPREM CNRS UMR 5254, Helioparc Pau Pyrénées, 2 Avenue de Président Angot, F-64053 Pau Cedex 9, France, and* [⊥]*University of Geneva, Laboratory of Crystallography, 24 Quai Ernest-Ansermet, CH-1211 Geneva 4, Switzerland*

Received October 5, 2009

The crystal structure of the new $Li_{5.5}Ce_{12}F_{50}$ compound has been fully characterized by single-crystal and synchrotron powder X-ray diffraction. An accurate pseudotetragonal structure was described in the monoclinic $P2_1$ space group with 68 independent crystallographic sites. The $Li_{5.5}Ce_{12}F_{50}$ composition belongs to the $Li_{2+x}Ce_x^{3+}Ce_{12-x}^{4+}F_{50}$ solid solution. Its structure consists of an opened fluorine framework where a channel network allows the intercalation of relatively mobile lithium cations, inducing the formation of the mixed-valence cerium (the intercalation of Li^+ leads to the reduction of a part of Ce^{4+} to Ce^{3+}). One part of the lithium ions, necessary for the electroneutrality of the tetravalent equivalent cerium fluoride ($Li_2Ce_{12}F_{50}$ composition), is in a locked fluorine polyhedron. Only the supplementary x amount of lithium is able to be exchanged in $Li_{2+x}Ce_x^{3+}Ce_{12-x}^{4+}F_{50}$. The structure of $Li_{2+x}Ce_x^{3+}Ce_{12-x}^{4+}F_{50}$ is a rearrangement, due to lithium intercalation, of the base CeF_4 structure. Bond valence calculation on Ce sites, Ce coordination polyhedra volumes, and a calculated Ce cationic radius give the indication of a partial long-range ordering of trivalent and tetravalent cerium cations in specific slabs of the structure. ^{7}Li NMR spectroscopy and XPS analyses have confirmed all of the structure details.

1. Introduction

In spite of their usual "rare earths" name, the lanthanide elements are now largely used in advanced technologies. The applications relate to optics with the development of solid lasers, optical fibers for telecommunications, and devices with electrochromic or electroluminescent diodes and so on. The remarkable magnetic properties of some inorganic fluorides result also in interesting potentialities. The diversity and the high added value of these applications justify the numerous research projects undertaken on these lanthanides and actinides fluorides. In particular, the crystal chemistry of terbium fluorides has been extensively studied because of the half-filled shell of the $4f^7$ electronic configuration of terbium, which stabilizes the tetravalent cation. Compounds exhibiting mixed valences are subject to many studies because of their potential applications related to the electronic exchange and magnetism.

Contrary to the cerium ions for which the +4 oxidation state can be stabilized in solution, the Tb^{4+} cation exhibits a high instability, justifying the low number of studies on tetravalent terbium compounds.[1−4] Nevertheless, Tb^{4+} is more easily stabilized by fluorine anions than by oxide anions. The tetravalent Ce^{4+} cation can be stabilized in either an oxygenated or fluorinated medium.[5−7] Up to now, very few mixed-valence terbium fluorides were reported in the literature. Among them, the Tb_4F_{15} compound was synthesized by Brekhovskikh et al.[8] and characterized by Popov et al.[9] Other mixed-valence terbium fluorides have

*To whom correspondence should be addressed. Tel.: 00 33 4 73 40 73 36. Fax: 00 33 4 73 40 71 08. E-mail: guillaume.renaudin@ensccf.fr.

(1) Cunningham, B. B; Fray, D. C.; Rollier, M. A. *J. Am. Chem. Soc.* **1954**, *76*, 3361–3363.
(2) Hoppe, R.; Rödder, K. M. *Z. Anorg. Allg. Chem.* **1961**, *312*, 277–278.
(3) Avignant, D.; Cousseins, J.-C. *C. R. Acad. Sci. Paris, Ser. C* **1974**, *278*, 613–616.
(4) Avignant, D.; Cousseins, J.-C. *Rev. Chim. Miner.* **1978**, *15*, 360–367.
(5) Laligant, Y.; Le Bail, A.; Ferey, G.; Avignant, D.; Cousseins, J.-C. *Eur. J. Solid State Inorg. Chem.* **1989**, *25*, 551–563.
(6) El-Ghozzi, M.; Avignant, D.; Cousseins, J.-C. *Eur. J. Solid State Inorg. Chem.* **1992**, *29*, 981–992.
(7) Gaumet, V.; Avignant, D. *Acta Crystallogr., Sect. C* **1997**, *C53*, 1176–1178.
(8) Brekhovskikh, M. N.; Popov, A. I.; Yu, M.; Il'inskii, A.; Fedorov, V. A. *Russ. J. Inorg. Chem.* **1989**, *34*, 573–577.
(9) Popov, A. I.; Val'kovskii, M. D.; Fedorov, P. P.; Yu Kiselev, M. *Russ. J. Inorg. Chem.* **1991**, *36*, 476–480.

 Published on Web 12/18/2009

been synthesized and characterized in our laboratory: KTb_3F_{12}[10,11] and $K_2Tb_4F_{17}$[12] present a long-range ordering between Tb^{3+} and Tb^{4+}. For others, such as the aluminum-containing terbium fluoride $Rb_2AlTb_3F_{16}$[13] and $RbAl_2Tb_4F_{22}$,[14] Tb^{3+} and Tb^{4+} are statistically distributed into the same crystallographic sites. Mixed-valence ternary terbium fluoride appears at a molar ratio of $TbF_4/AF > 1$ (A = Li, K, Rb, Cs). Chilingarov et al.[15] showed that the decomposition of TbF_4 into TbF_3 and atomic fluorine occurs at temperatures higher than 550 °C, even in a fluorine atmosphere. If the synthesis conditions allow it, TbF_4 in excess transforms to trivalent fluoride by decomposition, which is suitable to immediately combine with the other components of the reactive mixture. This forms Tb^{3+}/Tb^{4+} mixed-valence terbium fluoride. In other words, a thermally induced transformation occurs from the $AF-TbF_4$ binary system into the $AF-TbF_3-TbF_4$ ternary system. The obtained mixed-valence compounds are thermodynamically stable. Nevertheless, the reaction temperature and the cooling rate must be optimized. Thus, the terbium fluoride initially formulated, KTb_2F_9 ($TbF_4/KF = 2$), is actually a mixed-valence compound with the $K_2Tb_4F_{17}$ formula, that is, $K_2Tb^{3+}Tb^{4+}{}_3F_{17}$.[11]

In the $LiF-MF_4$ (M = Ce, Th, and U) binary systems, compounds formulated as LiM_4F_{17} were reported,[16−19] but no structural study confirmed their real stoichiometries. By analogy with terbium tetrafluorides, their location above the MF_4/LiF molar ratio equal to unity increases the ambiguity about their real stoichiometry. Indeed, the initial "$LiTh_4F_{17}$" composition has been corrected as $Th_6F_{24}\cdot H_2O$, a hydrated thorium tetrafluoride, thanks to a structural study which has been carried out on a single crystal by Cousson et al.[19] Nevertheless, these authors mentioned that lithium ions are necessary for the synthesis of the hydrated tetrafluoride, although they are absent from the structure.

With the dual aim of unambiguously determining the real stoichiometry of the "LiM_4F_{17}" (M = Ce, Th, and U) compounds and investigating whether the mechanism of formation of mixed-valence terbium fluorides is transposable to LiF/MF_4 systems, a compound of nominal composition 1LiF, $1CeF_3$, and $3CeF_4$ was synthesized and characterized. The synthesized $Li_{5.5}Ce_{12}F_{50}$ compound has a pseudotetragonal symmetry. A first paper describes the weak monoclinic distortion of the lattice.[20] The present paper gives its complete crystallographic description together with a ^{7}Li magic-angle spinning (MAS) NMR investigation. The mixed valence has been investigated by XPS experiments in order to extract the Ce^{4+}/Ce^{3+} ratio.

2. Experimental Section

2.1. Synthesis. Samples, used for single-crystal and synchrotron powder measurements, were synthesized by solid-state reactions involving a mixture of LiF (0.058 g), CeF_3 (0.444 g), and CeF_4 (1.459 g) starting materials in a 1:1:3 ratio. Pure CeF_4 tetrafluoride has been prepared by the following route: (i) dissolution of CeO_2 in a HF solution (40%), (ii) after evaporation of the solution, the dried resulting powder was fluorinated under a pure F_2 gas stream at 500 °C. CeF_3 was a commercial product (99.9% Aldrich). LiF (99.9%, Aldrich) was dehydrated by heating at 110 °C overnight in a primary vacuum. The 1:1:3 mixture was loaded into a platinum capsule (40 mm of length, 5 mm of diameter). The airtight platinum capsule was heated at 300 °C for 24 h, and then a temperature of 550 °C was applied over 72 h.

2.2. X-Ray Diffraction. Single-crystal X-ray diffraction intensity data were collected from two orange single crystals at room temperature by the use of a Stoe IPDS II image plate diffractometer. Both data were similar. The data set from the crystal given the best R_{int} was used to solve and refine the structure. The details of data collection and structure refinement are given in Table 1.

Synchrotron powder diffraction data of a freshly synthesized compound was obtained at the Swiss−Norwegian Beamline (SNBL) at the ESRF Grenoble (six analyzer crystal detector). More details are given in Table 1. Synchrotron powder diffraction was used to check the symmetry of the compound, that is, the weak lattice distortion unresolved with the image plate diffractometer. More details are given in ref 20.

2.3. ^{7}Li MAS NMR Spectroscopy. The ^{7}Li and ^{1}H spectra were recorded with magic angle spinning at room temperature using a Bruker MSL300 spectrometer operating at frequencies of 116.6 and 300.1 MHz for ^{7}Li and ^{1}H nuclei, respectively. The spinning rate was equal to 14 kHz using a 4 mm Bruker probe. A single $\pi/2$ pulse sequence was used (τ-acquisition with τ = 6 and 5 μs for ^{7}Li and ^{1}H nuclei, respectively). A total of 1000 and 128 scans were recorded with a recycling time of 1 and 5 s for ^{7}Li and ^{1}H, respectively. The ^{1}H chemical shift refers to tetramethylsilane by using adamantane as an external reference. The ^{7}Li chemical shifts are given with respect to solid LiCl.

2.4. XPS. XPS measurements were carried out with a Kratos Axis Ultra spectrometer using focused monochromatized Al Kα radiation ($h\nu$ = 1486.6 eV). For the Ag $3d_{5/2}$ line, the full width at half-maximum (fwhm) was 0.58 eV under the recording conditions. The analyzed area of the samples was 300 × 700 μm^2. Peaks were recorded with a constant pass energy of 20 eV. The pressure in the analysis chamber was ca. 5×10^{-8} Pa. To prevent the samples from moisture/air exposure on the analysis site, the XPS spectrometer was directly connected through a transfer chamber to a nitrogen drybox. Short acquisition time control spectra were recorded at the beginning and at the end of each experiment to check the nondegradation of the samples. The binding energy scale was calibrated from the carbon contamination using the C 1s peak at 285.0 eV. Core peaks were analyzed using a nonlinear Shirley-type background.[21] The peak positions and areas were optimized with a weighted least-squares fitting method using 70% Gaussian/30% Lorentzian lineshapes. Quantification was performed on the basis of Scofield's relative sensitivity factors.[22]

3. Structure Solution and Refinement

3.1. Structure Solution from Single-Crystal Data. A reciprocal lattice observed from both single crystals

(10) Avignant, D.; Largeau, E.; Gaumet, V.; Dugnat, P.; El-Ghozzi, M. *J. Alloys Compd.* **1998**, *275−277*, 1–5.
(11) Largeau, E.; El-Ghozzi, M.; Avignant, D. *J. Sol. State Chem.* **1998**, *139*, 248–258.
(12) Largeau, E. Ph.D. Thesis, Blaise Pascal University, Clermont-Ferrand, France, **1998**.
(13) Josse, M.; Dubois, M.; El-Ghozzi, M.; Avignant, D. *Solid State Sci.* **2003**, *5*, 1141–1148.
(14) Josse, M.; Dubois, M.; El-Ghozzi, M.; Avignant, D. *J. Alloys Compd.* **2004**, *374*, 213–218.
(15) Chilingarov, N. S.; Rau, J. V.; Sidorov, L. N.; Bencze, L.; Popovic, A.; Sukhoverkhov, V. F. *J. Fluorine Chem.* **2000**, *104*, 291–295.
(16) Thoma, R. E.; Insley, H.; Landau, B. S.; Friedman, H. A.; Grimes, W. R. *J. Phys. Chem.* **1959**, *63*, 1266–1274.
(17) Barton, C. J.; Friedman, H. A.; Grimes, W. R.; Insley, H.; Moore, R. E.; Thoma, R. E. *J. Am. Ceram. Soc.* **1958**, *41*, 63–69.
(18) Cousson, A.; Pages, M.; Cousseins, J. C.; Vedrine, A. *J. Cryst. Growth* **1977**, *40*, 157–160.
(19) Cousson, A.; Pages, M.; Chevalier, R. *Acta Crystallogr., Sect. B* **1979**, *35*, 1763–1765.
(20) Renaudin, G.; Mapemba, E.; El-Ghozzi, M.; Dubois, M.; Avignant, D.; Černý, R. *Z. Kristallogr.* **2007**, *26*, 455–460.
(21) Shirley, D. A. *Phys. Rev. B* **1972**, *5*, 4709–4714.
(22) Scofield, J. H. *J. Électron Spectrosc. Relat. Phenom.* **1976**, *8*, 129–137.

Table 1. Parameters of Data Collection and Treatment for Single-Crystal and Powder Sample of $Li_{5.5}Ce_{12}F_{50}$

	single crystal used for solution and refinement	powder used for lattice determination
formula	$Li_{5.5}Ce_{12}F_{50}$	
molar mass (g/mol)	2669.61	
space group	$P2_1$	
a [Å]	8.855(2)	8.82391(7)
b [Å]	22.968(5)	22.9188(2)
c [Å]	8.855(2)	8.85384(7)
β [deg]	90.0(−)	90.6093(2)
V [Å^3]	1800.94(2)	1790.44(3)
Z	2	
wavelength [Å]	0.71073 (Mo Kα)	0.37504
μ [mm^{-1}]	8.63	1.40
cryst size [mm]	0.103 × 0.095 × 0.060	0.2 glass capillary diameter [mm]
absorption correction	numerical from crystal shape and size	analytical for cylindrical shape
density (calcd) [g cm^{-3}]	4.92	4.95
data collection	Stoe IPDS II	SNBL powder diffractometer
detector distance [mm]	100	0.002 2θ step [deg]
exposure time [min]	3	0.5 time/step [s]
ω range; increment [deg]	0−180; 1.0	
2θ interval [deg]	2.29−59.53	1.0−17.5
range in hkl	$h = \pm 12$; $-28 < k < +31$; $l = \pm 12$	
reflns measured	15972	
reflns unique	8776	
R_{int}	0.042	
reflns with $I > 4\sigma(I)$	6312 ($R_\sigma = 0.039$)	
data/params	19.3	
structure solution	SIR92[8] SHELXS-97 (Sheldrick, 1997a)	
structure refinement	SHELXL-97 (Sheldrick, 1997b)	FullProf.2k [10]
S	1.51	13.8 χ^2
R_F (all reflns)	0.075	0.040 R_B (all reflections)
R_{wF}^2 (all reflns)	0.142	0.072 R_{wp} (background corrected)
extinction coefficient	0.00049(3)	
residual in difference electron-density map	−3.43, 2.63	

indicates a tetragonal lattice with $a = 8.855\,(2)$ Å and $c = 22.968(5)$ Å. Analysis of the diffraction data set underlines a 91% probability of a centrosymmetric structure with the $4/m$ Laue symmetry ($R_{int} = 0.061$) and a primitive lattice. Automatic analysis of the extinction conditions using the Autostart Module of WinGX[23] did not lead to the determination of the space group. The first attempt to solve the structure was performed in the $P4_2/n$ space group. The starting atomic parameters of heavy cerium atoms were deduced from an automatic interpretation of direct methods with SIR92.[24] Fluorine atoms were subsequently located from difference Fourier maps, and the structure was refined using SHELXL97.[25] The solution obtained in the $P4_2/n$ space group seemed to be correct (with $R = 0.197$), but refinement did not decrease below $R_F = 0.159$. Lithium atoms were not located in the structure by Fourier difference maps, and the refined composition corresponded to CeF_4 (all cerium atoms in an eight-fluorine coordination with a square-based antiprism neighboring). Refinement of the solution obtained with the $P\bar{4}$ space group brought a weak improvement with an $R_F = 0.154$ and a refined composition of $CeF_{4.167}$. Nevertheless, lithium atoms were not located, and all cerium atoms presented a disordered nine-fluorine coordination. Finally, the best solution was found in the $P4_1$ space group, and refinement led to $R_F = 0.083$, $R_{wF} = 0.155$, and $S = 1.49$. Lithium atoms were located by Fourier difference maps. The structure refinement was acceptable with a refined composition of $Li_2Ce_6F_{25}$, with two-thirds of cerium atoms coordinated in 8-fold coordination and one-third in 9-fold coordination. Because of the presence of some observed but normally systematically absent reflections, and the presence of numerous inconsistent equivalents, a supplementary resolution work was performed in monoclinic $2/m$ Laue symmetry ($R_{int} = 0.053$). After transformation of the diffraction data set in a monoclinic lattice with unique axis $\vec{b}$ (instead of the measured $\vec{c}$), the Autostart Module of WinGX[23] assigned the centrosymmetric $P2_1/c$ space group, but solution in this $P2_1/c$ symmetry was not acceptable. Finally, the structure of this new fluoride compound was solved and refined in the noncentrosymmetric $P2_1$ space group with a final $R_F = 0.050$ and a final refined composition of $Li_{5.5}Ce_{12}F_{50}$, indicating the presence of the Ce^{4+}/Ce^{3+} mixed valence.

3.2. Synchrotron Powder Diffraction. Synchrotron powder diffraction data have been recorded on a freshly prepared powdered sample in order to check the monoclinic symmetry of the lattice. Numerous diffraction line splittings were observed, clearly indicating a lowering of the previously supposed tetragonal lattice. Figure 1 shows the synchrotron powder diffraction data and Rietveld

(23) WinGX, version 1.70.01: Farrugia, L. J. *J. Appl. Crystallogr.* **1999**, *32*, 837−838.
(24) SIR92: Altomare, A; Cascarano, G.; Giacovazzo, C.; Gualiardi, A. *J. Appl. Crystallogr.* **1993**, *26*, 343−350.
(25) Sheldrick, G. M. *SHELXL-97*, release 97-2; University of Goettingen: Goettingen, Germany, 1997.

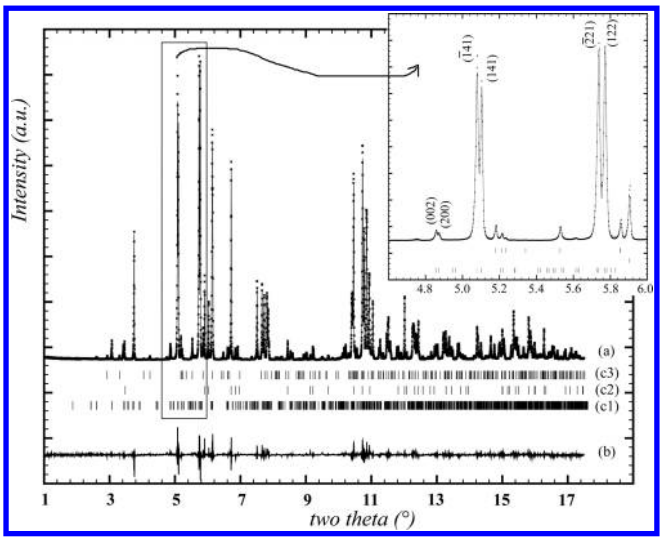

Figure 1. Rietveld plot of the fluoride sample (R_{wp} = 0.117 and χ^2 = 13.7 for global contributions, R_{Bragg} = 0.040 and R_F = 0.046 for the new fluoride phase). Observed (a, dots) and calculated (a, solid line) synchrotron (SNBL) powder diffraction pattern (λ = 0.37504 Å) are shown with a difference curve (b) and Bragg peak positions for $Li_{2+x}Ce_{12}F_{50}$ (c1; 83(1) refined weight %) and impurities CeF_3 (c2) and CeF_4 (c3). The inset shows the splitting from the monoclinic distortion of the lattice.

plot performed with FullProf[26] by using the atomic positions from the single-crystal data analysis ($P2_1$ symmetry). Refined monoclinic lattice parameters are a = 8.82391(7) Å, b = 22.9188(2) Å, c = 8.85384(7) Å, and β = 90.6093(2)°. Cerium trifuoride CeF_3 and cerium tetrafluoride CeF_4 impurities are present in the sample with, respectively, 13(1) and 4(1) refined wt %.

3.3. Structure Refinement. Structure parameters of $Li_{5.5}Ce_{12}F_{50}$ have been refined in the monoclinic $P2_1$ space group using single-crystal data. All relevant details concerning data collection and treatment are listed in Table 1. Structure solution has indicated 12 independent cerium positions. A total of 50 independent fluorine positions were subsequently easily discovered with Fourier difference maps. All of these atomic coordinates were refined (using full-matrix least-squares refinement on F^2) with anisotropic atomic displacement parameters for cerium atoms. Careful analysis of new Fourier difference maps, in accordance with geometric considerations, allowed the localization of lithium atoms. This led to six refined independent lithium atomic positions. In the final runs of refinement, two fluorine atomic displacement parameters were constrained to U_{iso} = 0.005 Å^2 because of an unrealistic quasi-zero refined value (F09 and F16). Due to similar geometric environments, Li1 and Li2 sites have been restrained to have the same atomic displacement parameter, as have the four similar Li3, Li4, Li5, and Li6 sites. Occupancy parameters have been checked for all of the atomic positions of the structure. The occupancy of the lithium position Li4 only deviated significantly from the unity at a value close to half occupancy. So, in the final run, its occupancy was fixed at 1/2, while all of the other sites were refined with the ideal occupancy corresponding to the composition $Li_{5.5}Ce_{12}F_{50}$ (Z = 2). The positional parameters of the 68 independent atomic positions of the structure are listed in Table SI1 (in the Supporting Information), and the anisotropic displacement parameters of cerium atoms are given in Table SI2 (in the Supporting Information). In the final run, 328 independent parameters were allowed to vary. Selected interatomic distances are listed in Table 2.

(26) Rodriguez-Carvajal, J. *FullProf.2k*, version 3.30; Laboratoire Léon Brillouin (CEA-CNRS): France, 2005.

4. Discussion

4.1. Structure Description. The structure of $Li_{5.5}Ce_{12}F_{50}$ is built from stacking of the cerium polyhedra with lithium cations inserted in cavities and channels. Figure 2 shows a general view of the structure along the [101] direction, and the projections of four details along the $\vec{b}$ monoclinic axis. Cerium atoms present two coordination numbers: 8-fold coordinated by fluorine for eight Ce sites (CN8 for Ce81 to Ce88 with a square antiprism polyhedron) and 9-fold coordinated by fluorine for four Ce sites (CN9 for Ce91 to Ce94 with a monocapped square antiprism polyhedron). Interatomic Ce−F distances, indicated in Table 2, are quite homogeneous around each Ce site: 2.20 Å ≤ d_{Ce81-F} ≤ 2.35 Å, 2.27 Å ≤ d_{Ce82-F} ≤ 2.39 Å, 2.22 Å ≤ d_{Ce83-F} ≤ 2.36 Å, 2.29 Å ≤ d_{Ce84-F} ≤ 2.45 Å, 2.09 Å ≤ d_{Ce85-F} ≤ 2.31 Å, 2.17 Å ≤ d_{Ce86-F} ≤ 2.36 Å, 2.10 Å ≤ d_{Ce87-F} ≤ 2.32 Å, 2.15 Å ≤ d_{Ce88-F} ≤ 2.31 Å, 2.12 Å ≤ d_{Ce91-F} ≤ 2.41 Å, 2.22 Å ≤ d_{Ce92-F} ≤ 2.45 Å, 2.14 Å ≤ d_{Ce93-F} ≤ 2.37 Å, and 2.22 Å ≤ d_{Ce94-F} ≤ 2.48 Å. Nevertheless, average Ce−F distances around each Ce site, or the volume of each Ce polyhedron, show three cases: Ce91 to Ce92 present a similar behavior corresponding to 9-fold Ce^{4+}, Ce85 to Ce88 present a similar behavior corresponding to 8-fold Ce^{4+}, and Ce81 to Ce84 present a gradual evolution (sequence Ce81, Ce83, Ce82, Ce84) corresponding to an 8-fold mixed valence (see Table 2 and Figure 3b). The calculated cerium cationic radius (considering the average Ce−F distances and an anionic radius of 1.285 Å for F^- [27]) agrees fairly well with these observations: around 0.96 Å for CN8 Ce^{4+}, around 1.01 Å for CN9 Ce^{4+}, and between 0.97 Å and 1.14 Å for CN8 mixed Ce^{3+}/Ce^{4+} (Figure 3a). These crystal chemical indications of the mixed valence correlate with the refined composition ($Li_{11}Ce_7^{3+}Ce_{17}^{4+}F_{100}$ per unit cell) and the orange color of our crystals. Bond valence sums (BVS[28]) have been calculated for cerium sites by considering the values of 2.036, respectively 1.995, for the bond valence parameter R_{ij} assuming Ce^{3+}, respectively Ce^{4+} (Table 2). Similar BVS calculations have been performed on CeF_3[29] and CeF_4[30] structures to validate the method. The calculated valences correlate well with our previous observations: tetravalent Ce^{4+} cations are located in the four 9-fold coordinated Ce91 to Ce94 sites and in the four 8-fold coordinated Ce85 to Ce88 sites; mixed Ce^{3+}/Ce^{4+} valences are located in the four 8-fold coordinated Ce81 to Ce84 sites. Polyhedra volumes, calculated cationic radii, and BVS calculations for the two Ce82 and Ce84 sites

(27) Shannon, R. D. *Acta Crystallogr. Sect. A* **1976**, *32*, 751–767.
(28) Brese, N. E.; O'Keeffe, M. *Acta Crystallogr., Sect. B* **1991**, *47*, 192–197.
(29) Cheetham, A. K.; Fender, B. E. F.; Fuess, H.; Wright, A. F. *Acta Crystallogr., Sect. B* **1976**, *32*, 94–97.
(30) Schmidt, R.; Mueller, B. G. *Z. Anorg. Allg. Chem.* **1999**, *625*, 605–608.

Table 2. Selected Interatomic Distances around Cerium Atoms, Polyhedron Volumes, and Bond Valence Sum Assuming Trivalent and Tetravalent Cerium Cations

					BVS		
central atom	fluoride ligands	distance (Å)	CN[a]	polyhedron volume (Å^3)	Ce^{3+}	Ce^{4+}	valence
Ce81[b]	F37	2.20 (2)			0.642	0.575	
	F47	2.20 (1)			0.642	0.575	
	F46	2.24 (2)			0.576	0.516	
	F48	2.25 (2)	8	20.47	0.561	0.502	III/IV
	F27	2.31 (2)			0.477	0.427	
	F04	2.33 (2)			0.452	0.404	
	F25	2.34 (2)			0.440	0.394	
	F42	2.35 (2)			0.428	0.383	
	<Ce81−F>	2.28			4.22	3.77	
Ce82	F43	2.27 (1)			0.531	0.476	
	F29	2.28 (1)			0.517	0.463	
	F18	2.29 (1)			0.503	0.451	
	F26	2.32 (2)	8	22.13	0.464	0.415	III
	F38	2.36 (1)			0.417	0.373	
	F07	2.37 (1)			0.405	0.363	
	F10	2.38 (1)			0.395	0.353	
	F12	2.39 (1)			0.384	0.344	
	<Ce82−F>	2.33			3.62	3.24	
Ce83[b]	F45	2.22 (2)			0.608	0.544	
	F35	2.23 (1)			0.592	0.530	
	F20	2.25 (1)			0.561	0.502	
	F44	2.29 (1)	8	20.77	0.503	0.451	III/IV
	F19	2.33 (2)			0.452	0.404	
	F17	2.35 (2)			0.428	0.383	
	F21	2.36 (2)			0.417	0.373	
	F15	2.36 (2)			0.417	0.373	
	<Ce83−F>	2.30			3.98	3.56	
Ce84	F41	2.29 (2)			0.503	0.451	
	F33	2.32 (2)			0.464	0.415	
	F24	2.32 (2)			0.464	0.415	
	F40	2.32 (2)	8	22.91	0.464	0.415	III
	F39	2.38 (1)			0.395	0.353	
	F13	2.40 (1)			0.374	0.335	
	F11	2.45 (1)			0.327	0.292	
	F08	2.45 (1)			0.327	0.292	
	<Ce84−F>	2.37			3.32	2.97	
Ce85	F11	2.09 (1)	8	19.49	0.864	0.774	IV
	F28	2.17 (1)			0.696	0.623	
	F16	2.24 (1)			0.576	0.516	
	F29	2.25 (2)			0.561	0.502	
	F46	2.25 (1)			0.561	0.502	
	F03	2.29 (2)			0.503	0.451	
	F22	2.31 (1)			0.477	0.427	
	F19	2.31 (2)			0.477	0.427	
	<Ce85−F>	2.24			4.72	4.22	
Ce86	F22	2.17 (1)			0.696	0.623	
	F13	2.20 (1)			0.642	0.575	
	F43	2.24 (1)			0.576	0.516	
	F48	2.25 (2)	8	19.93	0.561	0.502	IV
	F09	2.25 (1)			0.561	0.502	
	F30	2.28 (1)			0.517	0.463	
	F15	2.28 (2)			0.517	0.463	
	F05	2.36 (2)			0.417	0.373	
	<Ce86−F>	2.25			4.49	4.02	
Ce87	F10	2.10 (2)			0.841	0.753	
	F32	2.21 (1)			0.625	0.559	
	F41	2.21 (2)			0.625	0.559	
	F20	2.23 (1)	8	19.30	0.592	0.530	IV
	F04	2.24 (2)			0.576	0.516	
	F14	2.28 (1)			0.517	0.463	
	*F*23	2.30 (1)			0.490	0.439	
	F01	2.32 (2)			0.464	0.415	
	<Ce87−F>	2.24			4.73	4.23	
Ce88	*F*23	2.15 (1)			0.735	0.658	
	F07	2.20 (2)			0.642	0.575	
	F33	2.22 (2)			0.608	0.544	
	F44	2.25 (1)	8	19.39	0.561	0.502	IV
	F06	2.25 (1)			0.561	0.502	
	F25	2.26 (2)			0.546	0.489	
	F31	2.27 (1)			0.531	0.476	
	F02	2.31 (2)			0.477	0.427	
	<Ce88−F>	2.24			4.66	4.17	

Table 2. Continued

central atom	fluoride ligands	distance (Å)	CN[a]	polyhedron volume (Å^3)	BVS Ce^{3+}	BVS Ce^{4+}	valence
Ce91	F30	2.12 (1)			0.797	0.713	
	F08	2.15 (1)			0.735	0.658	
	F21	2.27 (2)			0.531	0.476	
	F03	2.31 (2)			0.477	0.427	
	F26	2.33 (2)	9	24.39	0.452	0.404	IV
	F34	2.35 (1)			0.428	0.383	
	F16	2.38 (1)			0.395	0.353	
	F49	2.40 (1)			0.374	0.335	
	F37	2.41 (2)			0.364	0.326	
	<Ce91−F>	2.30			4.55	4.07	
Ce92	F18	2.22 (1)	9	24.33	0.608	0.544	IV
	F34	2.23 (1)			0.592	0.530	
	F39	2.24 (1)			0.576	0.516	
	F17	2.24 (2)			0.576	0.516	
	F28	2.28 (1)			0.517	0.463	
	F05	2.30 (2)			0.490	0.439	
	F47	2.33 (1)			0.464	0.415	
	F09	2.43 (1)			0.345	0.309	
	F49	2.45 (1)			0.327	0.292	
	<Ce92−F>	2.30			4.50	4.02	
Ce93	F31	2.14 (1)			0.755	0.676	
	F12	2.14 (1)			0.755	0.676	
	F42	2.23 (2)			0.592	0.530	
	F01	2.31 (2)			0.477	0.427	
	F40	2.33 (2)	9	23.75	0.452	0.404	IV
	F35	2.33 (1)			0.452	0.404	
	F50	2.36 (2)			0.417	0.373	
	F36	2.37 (1)			0.405	0.363	
	F14	2.37 (1)			0.405	0.363	
	<Ce93−F>	2.29			4.71	4.22	
Ce94	F27	2.22 (2)			0.608	0.544	
	F36	2.22 (1)			0.608	0.544	
	F24	2.24 (2)			0.576	0.516	
	F38	2.24 (1)			0.576	0.516	
	F32	2.26 (1)	9	23.82	0.546	0.489	IV
	F45	2.29 (2)			0.503	0.451	
	F02	2.29 (2)			0.503	0.451	
	F06	2.40 (1)			0.374	0.335	
	F50	2.48 (1)			0.301	0.270	
	<Ce94−F>	2.29			4.60	4.11	

[a] Cerium coordination number. [b] Mixed valence cerium sites.

correspond to a trivalent Ce^{3+} cation (by comparison of the BVS values for Ce^{4+} and Ce^{3+} in Table 2).

The connection of the 8- and 9-fold coordinated polyedra forms an opened tridimentional framework. The structure is composed of a stacking of two kinds of slabs along the monoclinic axis. One kind of slab (labeled B and D in Figure 2 composed of Ce81 and Ce82 and of Ce83 and Ce84 polyhedra) is opened due to the presence of perpendicular channels along the [101] and [10$\bar{1}$] directions. Two-thirds of the lithium sites (Li3 and Li4 in slab B and Li5 and Li6 in slab D) are located at the crossing of this channel network. These lithium cations seem to be relatively mobile along the channels. The second kind of slab (labeled A and C in Figure 2, respectively composed by Ce85, Ce86, Ce91, and Ce92 and Ce87, Ce88, Ce93, and Ce94 polyhedra) is compact and contains locked lithium cations in the Li1 and Li2 sites, respectively in slab A and C. Off-center Li1 and Li2 sites are 8-fold-coordinated by fluorides. Compact A and C slabs are composed of tetravalent Ce^{4+} cations only. Each of these Ce polyhedra (Ce85 to Ce88 and Ce91 to Ce94) are linked to seven neighboring polyhedra (mainly corner- but also edge-sharing). The mixed valence cerium sites (Ce81 to Ce84) fully compose the opened B and D slabs. These cerium sites are in the vicinity of the mobile Li^+ sites (Li3 to Li6). A long-range ordering of Ce^{3+} and Ce^{4+} sites is then present in $Li_{1+x}Ce_6F_{25}$ (i.e., with a preferential location of Ce^{3+} in the four Ce81 to Ce84 sites when Li^+ cations are intercalated), as already observed in the Tb-based definite mixed-valence compounds KTb_3F_{12}[10,11] and $K_2Tb_4F_{17}$.[12] An explicit formula of the studied compound is $Li_{2+x}Ce_x{}^{3+}Ce_{12-x}{}^{4+}F_{50}$, indicating a minimum amount of lithium (two per unit formulas) and a progressive reduction of cerium (from Ce^{4+} to Ce^{3+}) when intercalating the x supplementary lithium cations.

The structure of $Li_{5.5}Ce_{12}F_{50}$ is related to CeF_4 (monoclinic $C2/c$ symmetry[20]). The CeF_4 structure presents a succession of opened and locked slabs also. "Opened" slabs in CeF_4 show similarity with the opened slabs B and D in $Li_{5.5}Ce_{12}F_{50}$. Locked slabs are different. They are composed of 8-fold coordinated Ce atoms only. Adjacent locked slabs are corner-sharing across the opened slab region, blocking the "opened" slabs. The $Li_{5.5}Ce_{12}F_{50}$ structure is a rearrangement of the CeF_4 structure, allowing the insertion of lithium cations into channels of the opened slabs. Large similitude with the

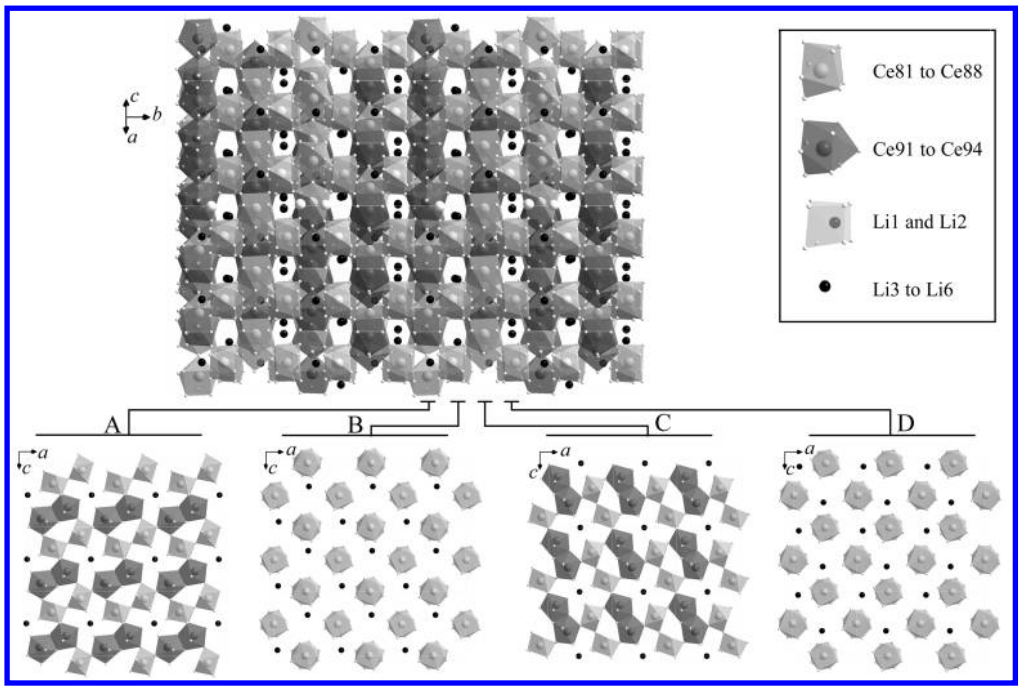

Figure 2. General representation (along [101]) and details (along [010]) of the $Li_{5.5}Ce_{12}F_{50}$ structure. Dark polyhedra and light polyhedra correspond respectively to cerium atoms with a CN9 and CN8 coordination number. Small white, large light gray, dark gray, and black balls correspond respectively to fluoride, cerium with CN8, cerium with CN9, and lithium atoms. Drawings A, B, C, and D are four details corresponding to the four independent structural slabs constituting the whole structure. The inset in the right top of the figure shows the fluoride neighboring of cations (coordination of lithium atoms, distorted cubic environment for Li1 and Li2, and bonds for Li3 to Li6 are not represented in the general and detailed views).

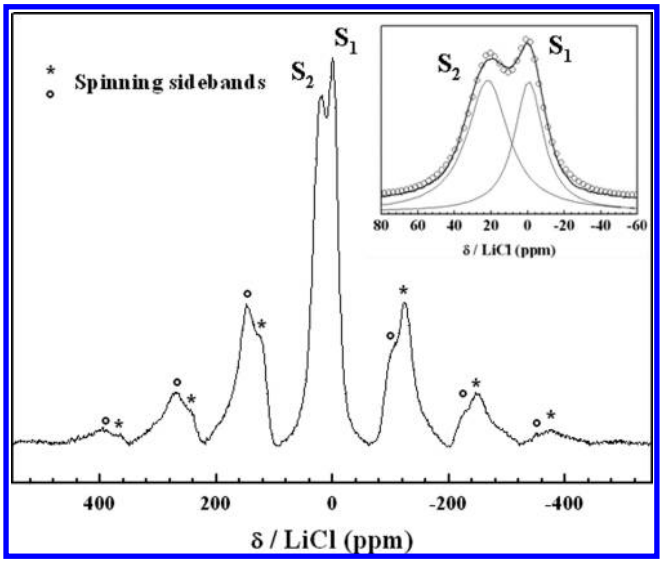

Figure 3. ^{7}Li MAS NMR spectrum of the $Li_{5.5}Ce_{12}F_{50}$ compound (spinning speed of 14 kHz, ○ and ∗ mark the spinning sidebands).

thorium fluoride $Th_6F_{24}\cdot H_2O$[16] is evidenced. The hydrate compound $Th_6F_{24}\cdot H_2O$, $I4/m$ symmetry, shows a similar network with all thorium cations 8-fold-coordinated (square antiprism) and water molecules located into the channel network of the opened slabs, at the location of the mobile lithium cations in the $Li_{5.5}Ce_{12}F_{50}$ structure.

The effective formation of a cerium mixed-valence fluoride is mainly supported by the refined Li^+ amount (which presents a large uncertainty due to its extremely weak scattering contrast, especially in the presence of cerium) and by crystal chemistry consideration (which are good indicators, but, in the present case, cannot be considered as definitive). The presence of two different environments for lithium cations has been checked with ^{7}Li MAS NMR spectroscopy, and the simultaneous presence of Ce^{3+} and Ce^{4+} has been investigated using XPS analysis (which allows qualitative and quantitative studies).

4.2. ^{7}Li NMR MAS Spectroscopy. Figure 4 displays the ^{7}Li NMR spectrum of the $Li_{5.5}Ce_{12}F_{50}$ compound. The NMR spectrum exhibits two peaks centered at 0 and 21.1 ppm noted S_1 and S_2, respectively, indicating the presence of two types of lithium ions. Although two types of lithium ions with different environments are highlighted by the structural study, the significant separation of the NMR lines is probably ascribable to the presence of Ce^{3+} paramagnetic ions, which results in the shift of the S_2 line. The paramagnetism effect on the chemical shifts has been discussed for lithium in several works, in particular for various compositions of the $Li(Ni,Co)O_2$ solid solution[31] and for nonstoichiometric $LiCoO_2$,[32] where the presence of the Ni^{3+} or Co^{2+} cations in the low spin state is accompanied by the appearance of new resonance lines in addition to the line at 0 ppm. Paramagnetic "external" species such as adsorbed oxygen molecules result in a shift for zeolites with a high silica content.[33] Considering the location of the Li^+ ions in the $Li_{5.5}Ce_{12}F_{50}$ structure, two-thirds of them (Li3, Li4, Li5, and Li6) are localized in the B and D layers, which contain

(31) Marichal, C.; Hirschinger, J.; Granger, P.; Menetrier, M.; Rougier, A.; Delmas, C. *Inorg. Chem.* **1995**, *34*, 1773–1778.
(32) Levasseur, S.; Menetrier, M.; Suard, E; Delmas, C. *Solid State Ionics* **2000**, *128*, 11–24.
(33) Accardi, R. J.; Lobo, R. F. *Microporous Mesoporous Mater.* **2000**, *40*, 25–34.

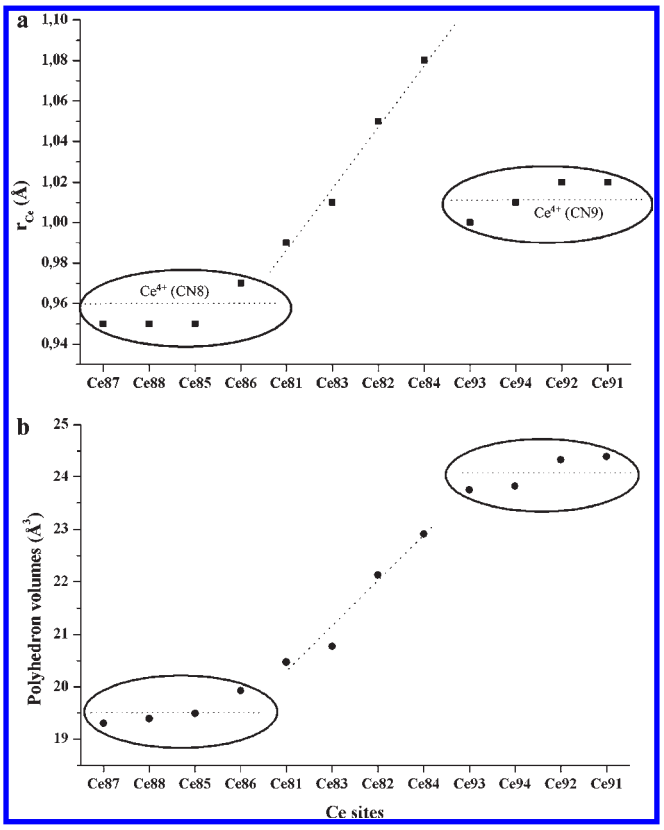

Figure 4. Environments of the 12 independent Ce sites: Calculated cerium ionic radius (a) and polyhedron volumes (b).

Ce^{3+} trivalent cerium ions. The other Li^+-including Li1 and Li2 ions are in the A and C layers, which are exclusively built with tetravalent cerium ions. One may assume that only the nuclear resonance of the first type of lithium is affected by the presence of paramagnetic Ce^{3+} because these ions are located within channels delimited by the mixed Ce^{3+}/Ce^{4+} ions in statistical distribution. In addition to the "paramagnetic" shift, the line width is also affected in the case of the S_2 line with a broadening; the fwhm's are equal to 2220 and 3170 Hz for S_1 and S_2, respectively.

Taking into account the assignment of the S_1 and S_2 lines and the number of involved lithium ions, the theoretical ratio of their integrated surfaces should be equal to 2:3.5, that is, 0.57. Indeed, even if the lithium nucleus is quadrupolar, integrated surfaces of the lines are almost proportional to the relative concentration of the Li^+ cations. The experimental ratio of 0.69 has been obtained by considering two Lorentzian lines for the fitting. The weak difference between the theoretical and experimental values could be explained by the particular structure of the compound. Indeed, the opened structure of $Li_{5.5}Ce_{12}F_{50}$ fluoride can be compared to an intercalation compound with stoichiometry $Li_{2+x}Ce_x^{3+}Ce_{12-x}^{4+}F_{50}$, where x can vary in large proportions. It is worthy of note that ^{1}H MAS NMR confirms the absence of water molecules within the opened channels of the $Li_{5.5}Ce_{12}F_{50}$ structure. As a matter of fact, no significant signal was obtained for its spectrum (not shown here).

4.3. X-Ray Photoelectron Spectroscopy (XPS). The more relevant peak to identify the simultaneous presence of Ce^{3+} and Ce^{4+} is the Ce3d core peak, located in the energetic window (Binding Energy), 880−920 eV. Note that XPS spectra of cerium compounds are known to exhibit rather complex features due to shake-up or -down lines, multiplet splitting or hybridization with ligand orbitals, and fractional occupancy of the valence 4f orbitals.[34] The Ce3d XPS spectrum of $Li_{5.5}Ce_{12}F_{50}$ (Figure 5) exhibits 10 components (labeled from 1 to 10) with the assignment of each component defined in Table 3. The theoretical basis for all of the components has been reported in the literature.[35]

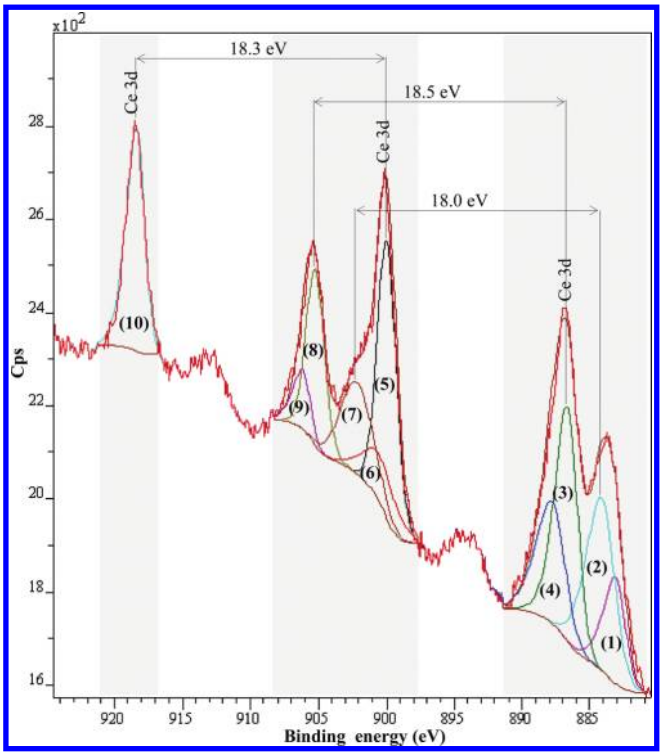

Figure 5. XPS Ce3d core level peaks of $Li_{5.5}Ce_{12}F_{50}$.

Table 3. Labeling and Mean Positions of the 10 Components of $Li_{5.5}Ce_{12}F_{50}$

		spin−orbit	characteristic	binding energy (eV)
Ce^{3+}	1	$3d_{5/2}$	shake down of 3	883.1
	6	$3d_{3/2}$	shake down of 8	900.5
	3	$3d_{5/2}$		886.7
	8	$3d_{3/2}$		905.2
	2	$3d_{5/2}$		884.2
	7	$3d_{3/2}$		902.2
Ce^{4+}	4	$3d_{5/2}$	satellite	887.7
	9	$3d_{3/2}$	satellite	906.2
	5	$3d_{5/2}$	satellite	900.0
	10	$3d_{3/2}$	satellite	918.4

Four peaks labeled 1 and 3 (for $3d_{5/2}$) and 6 and 8 (for $3d_{3/2}$) are related to the Ce^{3+} oxidation state. The satellite components 1 and 6 are related to the ligand-to-metal charge transfer phenomenon by the primary photoionization process. Six peaks labeled 2, 4, and 5 (for $3d_{5/2}$) and 7, 9, and 10 (for $3d_{3/2}$) referring to the three pairs of

(34) Shyu, J. Z.; Otto, K.; Watkins, W. L. H.; Graham, G. W.; Belitz, R. K.; Gandhi, H. S. *J. Catal.* **1988**, *114*, 23–33.
(35) (a) Fujimori, A. *J. Magn. Magn. Mater.* **1985**, *47*−*48*, 243–247. (b) Allen, J. W. *J. Magn. Magn. Mater.* **1985**, *47*−*48*, 168–174. (c) Fujimori, A. *Phys. Rev. B* **1983**, *28*, 2281–2283. (d) Fujimori, A. *Phys. Rev. B* **1983**, *27*, 3992–4001.

spin-orbit doublets are characteristic of Ce^{4+} final states.[36,37] The literature reports that the peak labeled 10 arises exclusively from Ce^{4+} due to a transition from the $4f^0$ initial state to the $4f^0$ final state. This fact is pretty interesting, as this component is isolated from the others and located around 918 eV. Then, this peak could be used as a quantitative probe of the amount of Ce^{4+}.[36,38,39] Indeed, it has been demonstrated that the integral area of the peak labeled 10 with respect to the total Ce3d area could be translated into the percentage of Ce^{4+}. The mean percentage of Ce^{4+} can be then calculated through the following relation:

$$Ce^{4+}\% = \frac{(10)\%}{14} \times 100$$

where (10)% is the percentage of the peak area corresponding to the component 10 with respect to the total Ce3d area. By using this formula, the experimental ratio Ce^{4+}/Ce^{3+} is equal to 1.75. By taking into account the refined weight amounts (13% for CeF_3 and 4% for CeF_4), we can reach the calculated formula $Li_{5.2}Ce_{3.2}{}^{3+}Ce_{8.8}{}^{4+}F_{50}$, very close to the refined one ($Li_{5.5}Ce_{3.5}{}^{3+}Ce_{8.5}{}^{4+}F_{50}$).

5. Conclusion

The structure of $Li_{5.5}Ce_{12}F_{50}$ has been successfully solved, refined, and described by combining single-crystal X-ray diffraction and high-resolution synchrotron powder diffraction data. The synchrotron powder diffraction pattern has been essential in determining the effective monoclinic $P2_1$ symmetry of the lattice, due to a weak distortion of a pseudo-tetragonal lattice. The structure of $Li_{5.5}Ce_{12}F_{50}$ is related to the structure of CeF_4,[14] with the intercalation of lithium cations allowed by opening a channel network. One part of Li^+ is locked, and the other part is relatively free to move along the channel network. The insertion of Li^+ into the channel leads to the reduction of one equivalent part of Ce^{4+} to Ce^{3+}. This is the first mixed-valence cerium fluoride. A long-range ordering of trivalent and tetravalent cerium cations has been observed. Structural details deduced from the crystal chemistry have been proven by spectroscopic analyses. The two kinds of Li^+ environments have been clearly identified by ^{7}Li NMR spectroscopy. And the presence of both Ce^{3+} and Ce^{4+} valences has been clearly established by XPS. The observed Ce^{4+}/Ce^{3+} ratio is in perfect agreement with the previously refined $Li_{5.5}Ce_{12}F_{50}$ composition. The structure description indicates that $Li_{1+x}Ce_{12}F_{50}$ is a good candidate to realize the electrochemical intercalation−disintercalation of Li^+ in order to change and to control the Ce^{3+}/Ce^{4+} ratio. Investigations are in progress.

Supporting Information Available: (Table SI1) Atomic positional and displacement parameters for $Li_{5.5}Ce_{12}F_{50}$. The equivalent isotropic displacement parameter U_{eq}, defined as one-third of the trace of the orthogonalized U_{ij} tensor, is given for cerium positions. (Table SI2) Anisotropic displacement parameters (pm^2) for cerium atoms in $Li_{5.5}Ce_{12}F_{50}$. This material is available free of charge via the Internet at http://pubs.acs.org.

(36) Holgado, J. P.; Alvarez, R.; Munuera, G. *Appl. Surf. Sci.* **2000**, *161*, 301–315.
(37) Pfau, A.; Schierbaum, K. D. *Surf. Sci.* **1994**, *321*, 71–80.
(38) Yu, X.; Li, G. *J. Alloys Compd.* **2004**, *364*, 193–198.
(39) Hughes, A. E.; Gorman, J. D.; Paterson, P. J. K. *Corros. Sci.* **1996**, *38*, 1957–1976.